

INVESTIGATION OF THE THERMOMECHANICAL BEHAVIOR OF A 2×2 TWILL WEAVE FABRIC ADVANCED TEXTILE COMPOSITE

A. Dixit,^{1*} H. S. Mali,² and R. K. Misra¹

Keywords: thermomechanical behavior, 2×2 twill weave, flat beam specimens, $\tan \delta$ curve, SEM

The thermomechanical performance of a 2×2 twill weave fabric advanced textile composite was evaluated. The tensile, compressive, and flexural properties of flat beam specimens of the composite were tested at room temperature, in water (24.9 to 96.7°C), and in liquid nitrogen (−96.9 to 99.4°C) by using a high-precision instrument called the dynamic mechanical analyzer (DMA). The storage modulus and $\tan \delta$ of the carbon-fiber-reinforced plastic (CFRP) specimens at various temperatures were evaluated. The scanning electron micrograph (SEMs) of deformed composite specimens revealed their failure mode (fiber pull-out, debonding, crack propagation, delamination, matrix cracking, and kinking of fibers).

1. Introduction

Composite materials are widely used in industry and various research areas due to their light weight, design flexibility, and processing ability [1], as their properties can be tailored to specific structural requirements. Polymer composites are engineering materials suitable for aerospace, automotive, and civil engineering structures because of their outstanding mechanical properties. The reinforcing materials employed most frequently are glass, carbon, and aramid, while polyethylene and boron are being used rarely. However, to offer new freedom to the design of structures and to improve their performance, fully interlaced fabrics comprising carbon fibers, termed advanced composites, are introduced. These composites have a potential for changing the way composite structures are designed and created [2]. Advanced composites have been universally accepted

¹School of Engineering, Department of Mechanical Engineering, Gautam Buddha University, Greater Noida, India, 201312

²Department of Mechanical Engineering, Malaviya National Institute of Technology, Jaipur, Rajasthan, India, 302017

*Corresponding author; tel.: +91-120-2346008; e-mail: anuragdixitiitd@gmail.com

by the engineering society, as they are manufactured from high-performance fibers pre-impregnated at a predetermined and controlled level in a matrix under the action of heat and pressure [3]. These materials exhibit a high strength and stiffness and a significant reduction in weight. Their high structural efficiency can be achieved by aligning fibers with the directions of principal stresses [4]. The foremost advantage of these fully interlaced yarn networks lies in their ability to increase the structural integrity and to reduce the risk of delamination, in enhanced through-thickness mechanical properties, in a reduced manufacturing cost, in an improved impact damage tolerance, and in an efficient transfer of internal loads [5]. These materials also possess an exceptional environmental and corrosion resistance, good vibration damping properties, an excellent fatigue life, and improved energy absorbing characteristics, and they can be used to manufacture items of a complex shape at a low cost [6]. In the recent past, many researchers [7-9] examined the thermomechanical characteristics of various polymer-based composites for their interfacial stress and strength. In this paper, attempts are made to evaluate the basic thermomechanical properties of advanced woven-fabric composites with a twill interlacing pattern. The mechanical properties of these composites can be engineered by altering weaving patterns, yarn tension, the types of warp and weft yarns, tow sizes, and fiber volume fractions in different directions.

2. Approach

The objective of the current investigation is to identify the fundamental mechanical properties of the 2×2 twill weave fabric composites on the material level in tension, compression, and bending as functions of time, temperature, and loading frequency. To do this, flat beam composite specimens with a rectangular cross section were tested on a sophisticated thermal analytical instrument known as the dynamic mechanical analyzer DMA. It measures the mechanical properties of materials as functions of time, temperature, and loading frequency and also analyzes their mechanical response to periodic stresses under varying thermal conditions in the presence of water and liquid nitrogen. The choice of the fabric mainly depends upon the weave type and thickness needed. The weave type is generally determined based on aesthetic and conformability requirements. The 2×2 twill weave provides the most dramatic look compared with that all other types of weave, while the conformability is connected with the adaptability of weaves to complex curves and with the ease of their fraying at edges [10]. The most flexible fabric is the twill weave ones, while the least conforming fabric is the plain weave one, because it is the tightest among all weaves [11-12]. Hence, it may be concluded that the looser a weave, the more conformable it will be to complex curves and the more easily it frays (at edges). Therefore, keeping in mind these facts, a 2×2 twill weave fabric composite was chosen as the material of interest for the present investigation.

Medium Temperature Mould MTM 28/280gsm woven carbon (CF0700) laminated plates of 2×2 twill pattern having eight plies of 0/90 configuration were obtained from Kineco Pvt. Ltd Goa, India. The tensile, compressive, and flexural properties of the laminates were determined, and the results obtained were analyzed. In this work the longitudinal direction is denoted by 1, the transverse direction by 2, and the out-of-plane direction by 3.

3. Experiments

Based on the systematic investigations carried out at the Institute of Polymer Mechanics of the Latvian Academy of Sciences [13-14] and the recommended test methods [15] suggested for the static mechanical testing of composites in tension, compression, and bending, flat beam specimens with a rectangular cross section were cut from the plates in order to evaluate the tensile, compressive, and flexural properties of the 2×2 twill weave fabric textile composite. Unless otherwise specified, five specimens per experiment were tested. All the tests were conducted on the dynamic mechanical thermal analyzer mentioned.

3.1. Tension test

The tension test was performed as per ASTM D5026 standard at a constant loading frequency of 1 Hz. The dimensions of tensile specimens were $5.10 \times 6.0 \times 0.80$ mm. The experiment was performed in the temperature/time scan mode by varying the temperature from 30 to 100°C with a heating rate of 5°C/min.

3.2. Compression test

The length, width, and thickness of compression specimens were 5.8, 10, and 8.15 mm, respectively, as per ASTM D5024. The compression experiment was conducted at a constant frequency of 1 Hz under the stress/strain scan. The temperature was varied from 23.6 to 45°C with a heating rate of 5°C/min.

3.3. Single cantilever bending test

Single cantilever bending is an excellent mode for the general characterization of the majority of polymer materials above and below their glass-transition temperature T_g . Dimensions of the specimens were $7.20 \times 9.34 \times 5.60$ mm. The experiment was performed in the creep mode at a constant frequency of 1 Hz. The temperature was varied from 24.2 to 105°C with a heating rate of 5°C/min. Usually, creep experiments are continued for many months or even years, but in this case, using the time-temperature superposition principle, the long-term behavior of the material could be predicted in a very short interval of time.

3.4. Dual cantilever bending test

This bending mode provides a simple means to characterize the thermomechanical behavior of plastic compositions by measuring their elastic and loss moduli as functions of time, temperature, or frequency. The dimensions of the specimens used in this test were $7.5 \times 8.70 \times 5.40$ mm, as per ASTM D5418 standard. In total, three tests were conducted. Initially, a thermomechanical analysis was performed under the time temperature scan mode at a constant frequency of 1 Hz. The temperature was varied from 27 to 95°C with a heating rate of 5°C/min. In order to evaluate the effect of moisture on the thermomechanical behavior of the material, the test was repeated in water at 25 to 97°C. In order to closely observe its cryogenic behavior during bending, the test was repeated in liquid nitrogen in the temperature range of -96 to +96°C. The damping property $\tan \delta$ and the storage modulus E_s were recorded at a certain temperature of interest in this mode.

3.5. Three-point bending test

The length, width, and thickness of specimens were 12.48, 8.67, and 5.54 mm, respectively. The test was performed as per ASTM D5023 standard under the strain scan mode, where the modulus and damping were recorded at an increased strain. The test was performed in the temperature range from 28.5 to 95°C with a heating rate of 5°C/min at a constant frequency of 1 Hz.

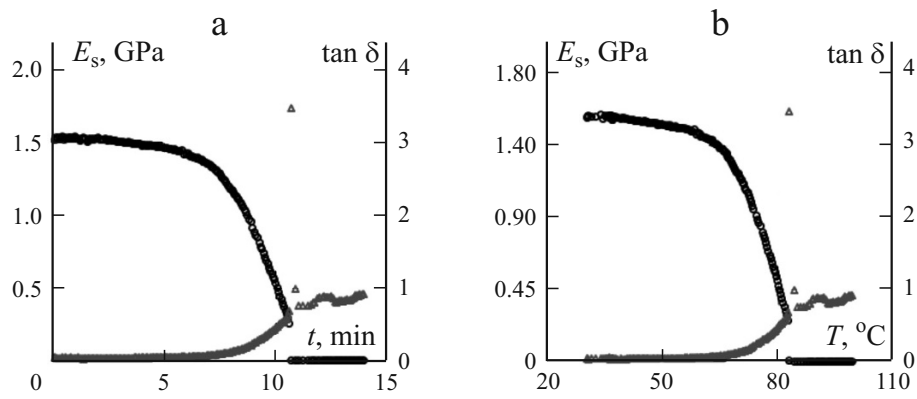


Fig. 1. Variations in the storage modulus E_s (\circ) and $\tan \delta$ (Δ) with time t (a) and temperature T (b) in the tension test.

4. Results and Discussion

Variations in the storage modulus E_s and $\tan \delta$ with respect to time t and temperature T are shown in Fig 1-7. The quantity $\tan \delta$, which is the measure of damping, characterizes the ability of a material to dissipate the mechanical energy by converting it into heat. Mathematically, it may be defined as the ratio of the loss modulus to the storage modulus. A study on the microstructure of the material was conducted based on images obtained from the scanning electron microscopy (SEM).

4.1. Tension test

Figure 1a, b shows the dynamic properties (E_s and $\tan \delta$) of the material in the tension mode as functions of time and temperature. Initially, up to 60°C, $\tan \delta$ remained constant and then increased continuously up to the target temperature 100°C. For the storage modulus, a continuous dip was observed from the start of test to the point of intersection with the $\tan \delta$ curve, and finally it tended to zero as the temperature approached 100°C. The glass-transition temperature T_g , which is defined by the peak in the $\tan \delta$ curve or by a great drop (a decade or more) in the storage modulus, see Fig. 1b, was found to be 84.2°C. In Figure 1a, it can be clearly seen that the damping parameter $\tan \delta$ initially remained almost constant up to six minutes and then increased gradually up to the end of test. For the storage modulus, a gradual dip from its initial value of 1.54 GPa to the final 1.06 MPa at $t = 14$ min was observed. In the thermomechanical analysis in the tension mode, a constant static force of 4.8 N was applied to the specimen, and the changes in material properties observed with variation in temperature are shown in Fig. 1b. The ratio control is generally the best tension control to use. It consists in applying a ratio of static force to the specimen based on the magnitude of the variable dynamic oscillating force required to obtain the amplitude assigned. A default value of the ratio equal to 1.5 was used in the present analysis. Before mounting a specimen in the fixture, an additional static force, or pretension, has to be applied to it, because the specimen cannot sustain the necessary level of compressive stresses. This pretension should be greater than the peak force attained in the dynamic oscillation, otherwise the specimen may suffer buckling, in which case the lower part of stress signal may get truncated. In short, the lower level of the static force, or pretension, should be greater than half of the peak value of the dynamic force in order to avoid the buckling mentioned. However, extra care should be taken in pretension, because an excessive static force at the beginning of the test may lead to permanent deformations of the specimen before its actual dynamic testing.

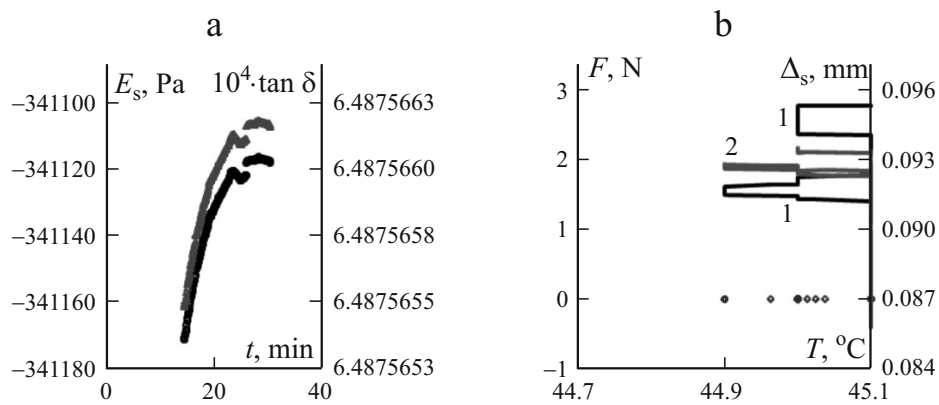


Fig. 2. Variations in E_s (\circ) and $\tan \delta$ (Δ) with time t (a) and in the static F_s (1) and dynamic F_d (\diamond) forces and static displacements Δ_s (\circ) with temperature T (b) in the compression test.

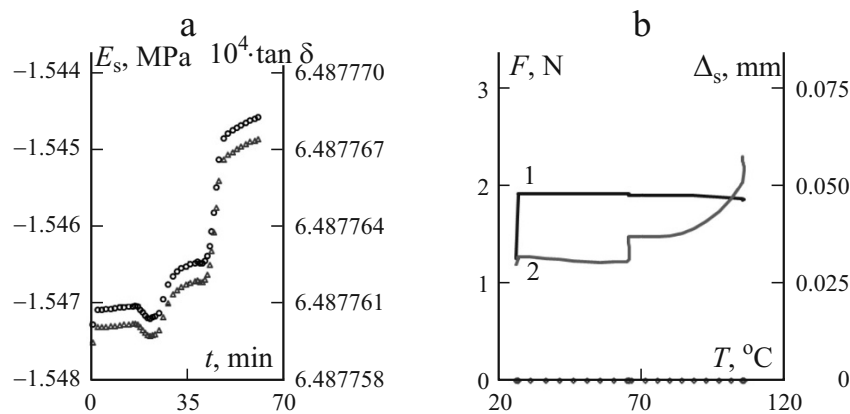


Fig. 3. The same in the single cantilever bending test.

4.2. Compression test

Variations in the dynamic properties (storage modulus E_s and $\tan \delta$) with time and temperature are shown in Fig. 2a. The records of storage modulus and $\tan \delta$ were taken in the interval of time from 14.4 to 30.3 min in an isothermal environment with $T = 45.1^\circ\text{C}$ in order to assess the behavior of the material at a certain temperature for a considerable period of time. The damping property $\tan \delta$ and the storage modulus were found to be constant with values of 0.006 and $3.41 \cdot 10^{-5}$ Pa, respectively, which clearly indicates that the material is able to sustain isothermal conditions. However, the static force increased from -0.208 to 2.772 N in the particular temperature interval. As expected, the static displacement did not vary much (from 0.086 to 0.093 mm), but the dynamic force was zero during the entire compression test, as shown in Fig. 2b.

4.3. Single cantilever bending test

The single cantilever bending test of the CFRP was performed in three different modes, namely in the creep, stress/strain, and T /time scans. The creep scan was performed to analyze the deformation of the material with time under a constant stress of 1.9 N in order to rapidly assess its long-term properties. The static stress/strain scan allowed us to find

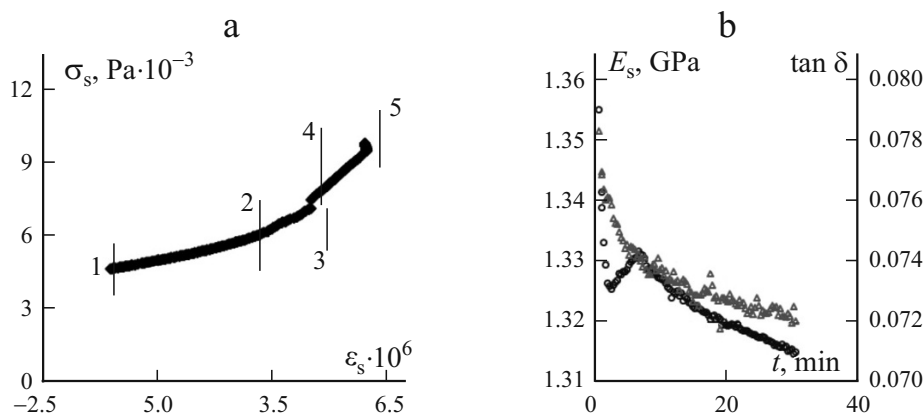


Fig. 4. The static stress–strain curve σ_s – ε_s (a) and variations in E_s (\circ) and $\tan \delta$ (Δ) with time t (b) in the cantilever bending test.

Young’s modulus and stress–strain curves, whereas the T/t scan characterized variations in T_g with increasing temperature at a constant loading frequency of 1 Hz.

During the creep scan, with temperature growing from 25.7°C to 105°C, it was observed that a very slight change (~0.002 MPa) in the storage modulus did not effect the damping factor $\tan \delta$, which indicated that the material was able to sustain prolonged loading at a higher temperature. The creep test was conducted for a period 1 h and 4 min. The static stress/strain scan gives the stress–strain curve, as shown in Fig. 4a. The specimen experienced compression at the start of the experiment due to the development of prestress during its clamping, which can be seen in the negative region of the static strain in the stress–strain curve. The value of the prestress was $4.69 \cdot 10^5 \text{ N/m}^2$, and the corresponding strain was 0.4%. Then, the stress gradually increased at a rate of 0.2 N/min. As shown in Fig. 4a, three different slopes (regions 1-2, 2-3, and 4-5) were observed. This can be explained by the fact that initially, when a small load was applied to the specimen, the force experienced by a fiber was transferred to the matrix. As the matrix, elongated more than the fiber, the greatest increase strain, as expected, was registered in region 1-2, as shown in Fig. 4a. Then, after the matrix transferred some amount of load to the fiber, the elongation rate of the composite specimen decreased. As the intensity of the load further increased, the adhesive bond between the matrix and fiber failed, the load was completely transferred to other fibers, and the slope of the stress–strain curve increased. The broken continuity of slope of the stress–strain curve may be attributed to a nonuniform distribution of matrix among fibers.

Figure 4b shows variations in the storage modulus E_s and $\tan \delta$ with time t in the simple T/t scan in the single cantilever bending test. As can be seen, the storage modulus decreased from 1.35 to 1.31 GPa, while the damping coefficient $\tan \delta$ decreased from 0.078 to 0.072. Thus the decline in the storage modulus can be attributed to changes in the glass-transition temperature T_g . This decline is a relative indicator of the degree to which a more ordered structural formation has taken place. However, withholding the modulus above T_g will subsequently result in lowering of the $\tan \delta$ peak.

4.4. Dual cantilever bending test

The dual cantilever bending mode was used to obtain information on the storage modulus above the glass-transition temperature T_g . The temperature/time scan of the specimen in the dual cantilever bending mode in terms of variations in the storage modulus and damping quantity $\tan \delta$ vs. temperature and time is shown in Fig. 5a, b. The storage modulus at the start of test, or at room temperature, was equal to 1.13 GPa, and then it gradually decreased to the final value of 1.05 GPa at the end temperature of 95°C. The storage modulus of the specimen at any random temperature, say 76°C, was found to be $1.12 \cdot 10^9 \text{ Pa}$, while its loss modulus was equal to $1.18 \cdot 10^7 \text{ Pa}$. In the present case, the value of $\tan \delta$ was found to be 0.010, which is in

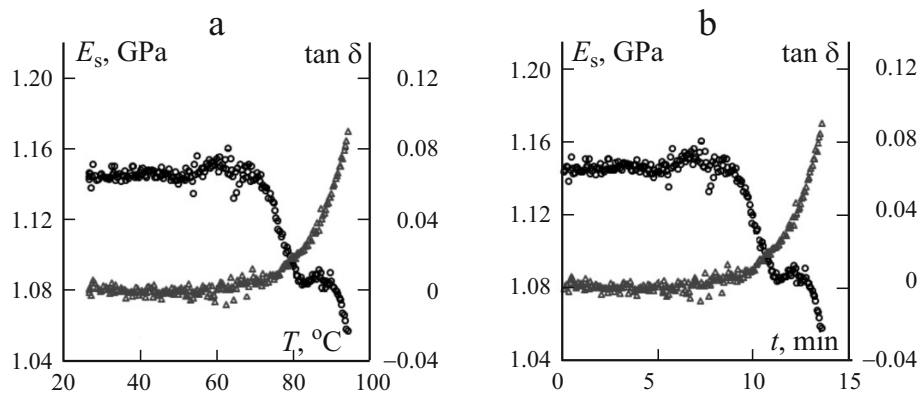


Fig. 5. Variations in E_s (\circ) and $\tan \delta$ (Δ) with temperature T (a) and time t (b) in the dual cantilever bending test.

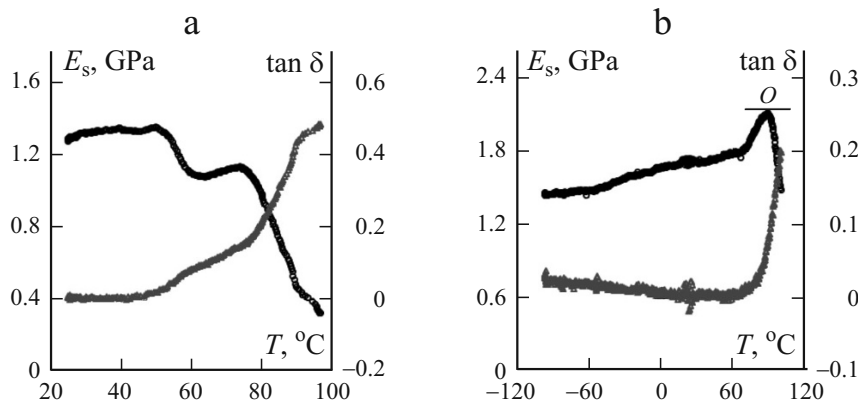


Fig. 6. Variation in E_s (\circ) and $\tan \delta$ (Δ) with temperature T in the dual cantilever tests of specimens immersed in water (a) and liquid nitrogen (b).

agreement with that directly obtained from the graph. In general, the top peak observed for $\tan \delta$ in conjunction with the relatively prominent drop in the storage modulus corresponds to T_g .

4.4.1. Water bath. Dry specimens were immersed in distilled water at room temperature for a certain period of time in a special attachment included in the DMA. Then, a double cantilever bending test was carried out up to the end temperature of 100°C in the temperature/time scan to visualize the hygroscopic behavior of the material. At the beginning of the test, the storage modulus was found to be $1.2 \cdot 10^9$ Pa. As soon as the test progressed in water, the storage modulus of the CFRP specimen decreased sharply to $3.2 \cdot 10^8$ Pa, as shown in Fig. 6a. This results indicates that water acted as a plasticizer on the polymer contained in the CFRP. A reverse effect was observed for the damping parameter $\tan \delta$, whose initial value of 0.009 increased with temperature to its peak value (~ 0.4) at about 100°C, at which the latent water had been driven off. However, a further increase in temperature resulted in melting of the specimen.

4.4.2 Liquid nitrogen. Figure 6b shows variations in the storage modulus E_s and $\tan \delta$ with temperature in liquid nitrogen. The test was conducted in the temperature range of -96.5°C - 100°C . At the low temperatures, the values of $\tan \delta$ were also very low, because the free volume of the polymer was so small that the movements of polymer segments hardly took place in the dynamic experiment and the dissipation of energy was weak. At $E_s = 2.1$ GPa, the polymer was in the glassy state. As the temperature increased, the movements of polymer segments also increased, and, after a certain level, the free volume of the polymer started to grow more rapidly than the volume expansion of molecules, thus facilitating the segmental motion. The temperature at which this phenomenon occurs is said to be the glass-transition temperature, T_g . From this point

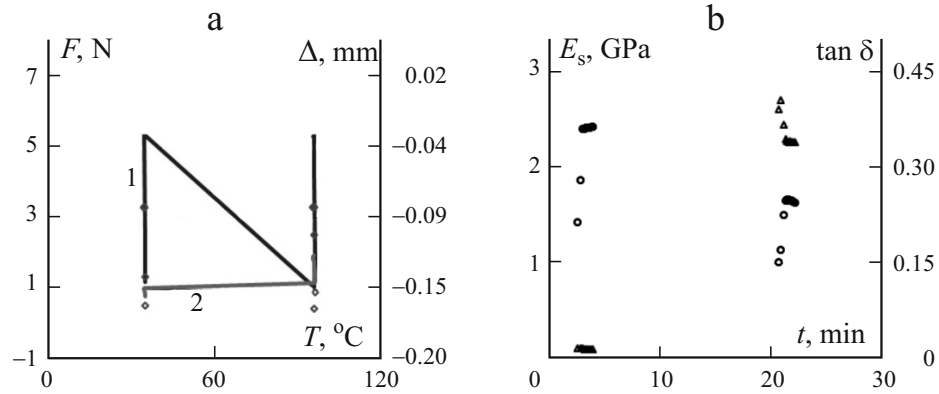


Fig. 7. Variation in the static force F_g (1), dynamic force F_d (Δ), and static displacement Δ_s (2) with temperature T (a) and in E_s (○) and $\tan \delta$ (Δ) (b) with time t in the three-point bending test.

on (marked as O in Fig. 6b), a drop in the modulus began, because the viscosity of the polymer decreased rapidly with increase in temperature, and the adjustment of molecules took place. However, on further increasing the temperature, a significant drop in the storage modulus was observed, because the brownian motion rapidly resulted in low viscosity and polymer molecules exhibited segmental motion, or low resistance to strain. Contrary to the behavior of the storage modulus, a continuous rise in $\tan \delta$ was observed until its peak was attained at almost 100°C temperature, which can be refer to as T_g .

4.5. Three-point bending test

For three-point bending, each specimen was heated from 35 to 95.4°C at a rate of 5°C/min, constant frequency of 1 Hz, and an initial static force of 1.2 N. The static force F sharply rose to 5.36 N with the corresponding modulus of $2.4 \cdot 10^9$ Pa and then rapidly dropped in the temperature range of 34-96°C, as shown in Fig. 7a. Then, the static force again sharply increased and ended with the value of 5.30 N.

As far as the storage modulus E_s and $\tan \delta$ are concerned, both were found to be showing opposite variations in relation to time/temperature, as seen in Fig. 7b. Initially, the storage modulus was equal to be $1.87 \cdot 10^9$ GPa at room temperature, and then it gradually increased until the temperature of 34°C was reached. At the end of the higher-temperature zone, at about 96°C, it finally decreased to $1.63 \cdot 10^9$ Pa. But the damping factor $\tan \delta$ increased with temperature until the stage of T_g was reached.

5. Scanning Electron Micrography (SEM)

In order to determine the failure mode and deformation pattern of the above-tested composites, scanning electron microscopy (SEM) images were collected. A SEM analysis was performed on a high-capacity ZEISS instrument. To prevent the distortion of specimen surface from high-intensity electron beams, the specimens were previously coated with a sputter coater (95% gold and 5% Pa). The coating was done in a separate chamber, where vacuum in the pressure range of 10^{-1} to 10^{-2} bar was created. The specimens in this chamber were mounted on a round plate to which initially a 1KV voltage was applied, resulting in heating of the plate. The value of current was kept at 20 mA for 150 s, which caused falling of the coating material in the form of rays on the specimens. The thickness of the coating was found to be 21 nm in the present investigation. From the woven carbon/epoxy composite plate manufactured, one fractured test specimen was taken for the SEM study.

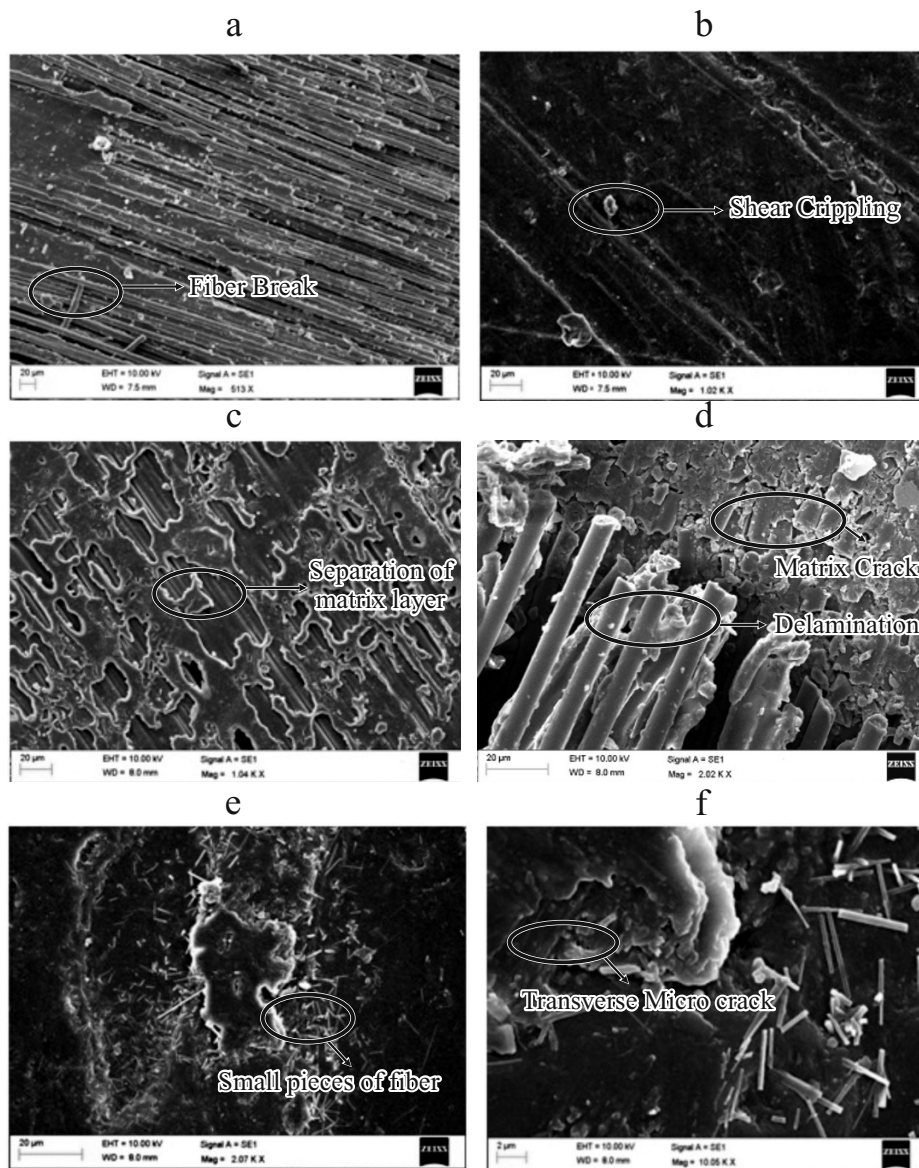


Fig. 8. SEM micrographs of woven carbon/epoxy specimens fractured in tension (a), compression (b), single cantilever bending (c), three-point bending (d), and dual cantilever bending in liquid nitrogen (e, f).

Figure 8a shows a SEM image of initiation and propagation of damage in a woven CFRP test specimen under the tension mode. Initially, the weakest sets of fiber bundles were found to be displaced and broken, which acted as stress concentrators for the initiation and propagation of damage under the tensile load. Later, with growing load, the damage tended to propagate into the matrix. The failure was more or less uniform so long as the pullout length was minimum. The direction of initiation and propagation of damage was identified through visual inspection and was further confirmed by examining the radial directions on individual fractured fibers. Under compression loading, the failure mode in the woven carbon/epoxy specimens was mainly found to be dependent upon the degree of fiber/matrix adhesion: at a relatively low degree, the mechanism could be global delamination buckling; at an intermediate degree, it could be fiber microbuckling; lastly, at a high degree of adhesion, it could be the compression (shear) failure of fibers. The shear crippling, shown in Fig. 8b, was identified as the predominant macroscopic failure in the present case due to the formation of kinking bands similar to the slip lines in the case of metals.

The SEM examination of test specimens revealed an irregular step structure at different locations of the specimens, consisting of several crushed and angled broken fibers. This irregular stepped structure was caused by the local buckling/kinking and fracture of fibers.

Figure 8c shows the SEM image of a woven carbon/epoxy composite specimen under creep in the single cantilever bending test. The failure initiated with separation of the matrix layer from fiber bundles, thereby creating a distinct gap followed by bending of fibers away from the fixed end. Figure 8d displays the SEM image of a specimen failed under three-point-bending. Here, two typical situations were observed, from matrix cracking to debonding, with increase in the fiber volume fraction. The matrix cracking was observed over all range of fiber volume fractions, which is an indication of a high transverse tensile strength. The delamination seems to be the governing failure mechanism here, which was caused by the presence of fiber bundles in the woven layers; however, the fiber-matrix interface appeared to be rather good.

The micrographs shown in Fig. 8e,f illustrates the failure pattern of composite specimens, after their cryogenic conditioning in liquid nitrogen, subjected to the dual cantilever bending. A few fiber breaks were found in the image, which were not common in transverse tensile failure surfaces unless and until the fibers were not misoriented. Due to the very low temperature, the fibers and matrix became brittle, resulting in an increased compressive strength and decreased tensile strength of the composites. However, all fibers retained a great deal of resin on their surface, indicating a strong interfacial bond, and primarily the failure mode was the failure of resin. The upper part of Fig. 8f shows the formation of a cup due to the development of transverse microcracks along the interfacial area. At lower temperatures, as the brittleness of the matrix was high, these microcracks opened easily and further formed the profile of a row of cups. Finally, when these cracks accumulated and merged to form a longitudinal crack along fibers, failure of the composite occurred.

7. Conclusions

The effect of temperature in various loading modes on the dynamic mechanical properties of a CFRP has been thoroughly studied using a sophisticated instrument, i.e., a dynamic mechanical analyzer. The present work was oriented to understanding the effect of temperature on the storage modulus, loss modulus, and the damping parameter $\tan \delta$ of the CFRP. The changes in its elastic and damping properties were determined by measuring the storage and loss moduli. In order to ascertain the functionality of the material at temperatures at which it is brittle, the material was tested for its strength and stiffness in liquid nitrogen. The microstructure of the material was closely examined for its microlevel properties by using a scanning electron microscope. The following conclusions were made from an analysis of the experimental results obtained:

- In the range of temperatures considered, which included the glass-transition process of the polymeric matrix, the CFRP was much more vulnerable in compression than in tension.
- The position and value of the $\tan \delta$ peak for each DMA mode was determined. The $\tan \delta$ peak provided a repeatable point of reference for measuring T_g , as the dimensions of specimens were not included. However, its value was always higher than that derived from the onset of transition measured by the storage modulus, which is directly related to the transition in stiffness of the material.
- The cryogenic conditioning of CFRP specimens in liquid nitrogen resulted in the development of residual stresses due to the different contraction of matrix and fiber at very low temperatures. These stresses developed at interfaces and were compressive in nature. The storage modulus was found to be maximum in the dual cantilever bending in liquid nitrogen. The composite specimens cooled in liquid nitrogen showed higher damping than the pure polymer.
- The cryogenic conditioning of woven carbon/epoxy composites in liquid nitrogen led to high residual stresses at interfaces, which caused massive cracking of matrix and interfacial debonding. The cryogenic conditioning stimulated the formation of rows of cups due to the coalescence of transverse microcracks, which led to the formation of longitudinal cracks along fibers.
- The overall strain-rate sensitivity of the laminate was mostly controlled by the resin. However, the anisotropic nature of carbon fibers played a vital role in the interlaminar shear strength of the laminate at cryogenic temperatures.

- For the specimens immersed in water, the moisture diffusion in the fiber direction was found to be much faster than in the transverse one. However, the number of transverse cracks and the delamination area of wet specimens was found to be smaller than those of dry specimens due to the softening of CFRP as a result of water absorption.
- From a series of experiments conducted over a range of temperatures, it was found that the damping of specimens could be kept within the limits of that of the polymer over any range of frequencies at low temperatures, and it was also possible at any temperature at higher frequencies, except for liquid nitrogen-cooled specimens.
- T_g of the subject material was found to be significantly above room temperature, because epoxy resins (matrix) are three-dimensionally cross-linked molecular structures. These structures were formed during the processing phase of composite, where the hardener or curing agent reacted and T_g increased from 50 to 300 K.
- From a SEM analysis, it was found that the pull-out of fibers, along with their separation from matrix, was the failure mode in tension. In compression, the failure depended on the strength of fiber/matrix adhesion. In three-point bending, matrix cracking and debonding dominated at various fiber volume fractions. In dual cantilever bending in liquid nitrogen, fiber breakage, massive matrix cracking, and interfacial debondings were observed due to the formation of high residual stresses.
- The results of the current investigation could find their application to aerospace structural components, where it is vital to access the extent to which each weave parameter has an effect on the thermomechanical behavior of woven-fabric laminates.

REFERENCES

1. Ch. M. Pastore, "Opportunities and challenges for textile reinforced composites," *Mech. Compos. Mater.*, **36**, No. 2, 97-116 (2000).
2. A. V. Roze and I. G. Zhigun, "Three-dimensional reinforced fabric materials. 1. Calculation model," *Polym. Mech.*, **6**, No. 2, 272-278 (1970).
3. A. Dixit and H. S. Mali, "Modelling techniques for predicting the mechanical properties of woven-fabric textile composites: A Review", *Mech. Compos. Mater.*, **49**, No. 1, 1-20 (2013).
4. W. L. Wu, M. Kotaki, H. Hamada, and Z. I. Maekawa, "Mechanical properties of warp-knitted, fabric-reinforced composites," *J. Reinforced Plastics and Composites*, **12**, No. 10, 1096-1110 (1993).
5. L. Tong, A. P. Mouritz, and M. K. Bannister, *3D Fiber Reinforced Polymer Composites*, Elsevier, ISBN: 0-08-043938-1, (2002).
6. M. Takeno, S. Nishijima, T. Okada, K. Fujioka, Y. Tsuchida, and Y. Kuraoka, "Thermal and mechanical properties of advanced composite materials at low temperatures," *Advances in Cryogenic Engineering Materials*, **32**, 217-224 (1986).
7. E. S. Molchanov, V. E. Yudin, K. A. Kydraliev and V. Yu. Elokhovskii, "Comparison of the thermomechanical characteristics of PORCHER carbon fabric-based composites for orthopaedic applications," *Mech. Compos. Mater.*, **47**, No. 3, 343-350 (2012).
8. S. Benyoucef, A. Tounsi, R. Yeghnem, M. Bachir Bouiadjra, and E.A. Adda Bedia, "An analysis of interfacial stresses in steel beams bonded with a thin composite plate under thermomechanical loading," *Mech. Compos. Mater.*, **49**, No. 6, 641-650 (2014).
9. N. K. Kucher, M. N. Zarazovskii, and E. L. Danil'chuk, "Deformation and strength of laminated carbon-fiber-reinforced plastics under a static thermo mechanical loading," *Mech. Compos. Mater.*, **48**, No. 6, 669-680 (2013).
10. A. Dixit, H. S. Mali, and R. K. Misra, "A Micromechanical unit cell model of 2x2 twill woven fabric textile composite for multi scale analysis," *J. of Institution of Engineers (India): Series E*, **95**, No. 1, 1-9 (2014).
11. N. Khokar, "3D fabric-forming process: distinguishing between 2D-weaving, 3D-weaving and an unspecified non-interlacing process," *J. Textile Inst.*, **87**, No.1, 97-106 (1996).
12. A. Dixit, R. K. Misra, and H.S. Mali, "Compression modeling of plain weave textile fabric using finite elements," *Materialwissenschaft und Werkstofftechnik*, **45**, No.7, 600-610 (2014).
13. V. Kalkis, R. D. Maksimov, M. Kalnins, J. Zicans, T. Bocoka, and O. Revjakin, "Thermomechanical and adhesive properties of radiation-modified polymer composites for thermosetting products," *Mech. Compos. Mater.*, **36**, No.3, 223-232 (2000).

14. E. Zile and V. Tamuzs, "Mode II delamination of a unidirectional carbon fiber/epoxy composite in four-point bend end-notched flexure tests," *Mech. Compos. Mater.*, **41**, No. 5, 383-390 (2005).
15. Yu. M. Tarnopol'skii and V. L. Kulakov, "Tests methods for composites — Survey of investigations carried out at the IPM of the Latvian Academy of Sciences in 1964-2000," *Mech. Compos. Mater.*, **37**, No. 5/6, 431-448 (2001).